Elasticity behavior, phonon spectra, and the pressure-temperature phase diagram of HfTi alloy: A density-functional theory study

Yong Lu[1] and Ping Zhang[1,*]

[1]*LCP, Institute of Applied Physics and Computational Mathematics, Beijing 100088, People's Republic of China*

Abstract

The pressure-induced phase transition, elasticity behavior, thermodynamic properties, and $P-T$ phase diagram of α, ω, and β equiatomic HfTi alloy are investigated using first-principles density-functional theory (DFT). The simulated pressure-induced phase transition of the alloy follows the sequence of $\alpha \rightarrow \omega \rightarrow \beta$, in agreement with the experimental results of Hf and Ti metals. Our calculated elastic constants show that the α and ω phases are mechanically stable at ambient pressure, while the β phase is unstable, where a critical pressure of 18.5 GPa is predicted for its mechanical stability. All the elastic constants, bulk modulus, and shear modulus increase upon compression for the three phases of HfTi. The ductility of the alloy is shown to be well improved with respect to pure Hf and Ti metals. The Mulliken charge population analysis illustrates that the increase of the d-band occupancy will stabilize the β phase under pressure. The phonon spectra and phonon density of states are studied using the supercell approach for the three phases, and the stable nature of α and ω phases at ambient pressure are observed, while the β phase is only stable along the [110] direction. With the Gibbs free energy calculated from DFT-parametrized Debye model as a function of temperature and pressure, the phase transformation boundaries of the α, ω, and β phases of HfTi are identified.

PACS numbers: 62.20.-x, 63.20.D-, 64.60.-i

*Author to whom correspondence should be addressed. E-mail: zhang_ping@iapcm.ac.cn

I. INTRODUCTION

Group-IV transition metals and alloys have attracted great scientific and technological interests since their particular applications in the aerospace, atomic energy industry, nuclear reactor, and chemical industry. The three Group-IV metals that occur naturally are titanium (Ti), zirconium (Zr) and hafnium (Hf). Titanium is recognized for its high strength-to-weight ratio with low density, meanwhile, the corrosion resistance, the heat stability, and the ductility are of benefit. The foremost use of hafnium and zirconium has been in nuclear reactors due to their corrosion resistance. Hafnium has a high thermal neutron-capture cross-section while zirconium possesses a rather low one, therefore, they can be used as control rod and cladding of fuel rods in nuclear reactors respectively [1–3]. Properly, hafnium and zirconium are used in nickel-based super alloys to improve their mechanical properties [4].

The titanium, hafnium and zirconium are complete solid solution between each other. The appropriate solution of these metals will help to improve the mechanical or thermal properties. Scientifically, most interests are attracted in their narrow d-band in the midst of a broad sp-band, where an increase in d-electron population by transfer from the s band is the driving force behind the structural and electronic transitions [5, 6]. The pressure-induced phase transformation sequence has received extensive experimental as well as theoretical attention [7–10]. At room temperature and under compression, Hf undergoes a crystallographic phase transition from hcp (α phase) to the hexagonal structure (ω phase) at about 38±8 GPa [9]. Upon further compression, Hf has been observed to transform into the bcc structure (β phase) at 71±1 GPa [9]. For Ti, the measured phase transition sequence at room temperature is $\alpha \rightarrow \omega \rightarrow \gamma \rightarrow \delta$ [10–13], and the β phase has not yet been observed up to 216 GPa [12]. However, the recent theoretical investigation [14] found that the δ phase is not stable under hydrostatic compression, and the δ phase should be replaced by β phase at zero Kelvin. The absence of the high-pressure β phase for Ti in experiments was attributed to the possible nonhydrostatic stress which distorts the β phasse [15].

The equilibrium phases at ambient pressure of the Hf-Ti system have been tabulated by several studies [16–20], containing the liquid, and the β and α phases of the solid. The $\alpha \rightarrow \beta$ phase transition for the equiatomic HfTi alloy has been measured to be ∼1200 K at ambient pressure. However, up to now, the effects of pressure on the phase transition of HfTi alloy have not been reported yet. The stability of the α, ω, and β phases of HfTi alloy also

need for testing to support their practical application. Thus, in the present study, our main task is to investigate the pressure-induced phase transition, the elasticity behaviors upon pressure, and the thermodynamic properties of equiatomic HfTi alloy. As well, the $P-T$ phase diagram are also predicted. The rest of the paper is organized as follows. The theory of Helmholtz energy calculation in the quasiharmonic approximation and computational details of first-principles are briefly introduced in Section II. The calculation results are presented and discussed in Section III. Finally, we give a summary of this work in Section IV.

II. THEORY AND CALCULATION METHODS

The Helmholtz free energy F can be approximated as

$$F(V,T) = E(V) + F_{vib}(V,T) + F_{ele}(V,T), \tag{1}$$

where $E(V)$ stands for the ground-state cold energy, $F_{vib}(V,T)$ is the vibrational energy of the lattice ions at a given unit cell volume V, and F_{ele} is the thermal electronic contribution to the free energy. Under quasihamonic approximation [21], the $F_{vib}(V,T)$ can be evaluated from phonon density of states (DOS) $g(\omega)$ by

$$F_{ph}(V,T) = k_B T \int_0^\infty g(\omega) \ln\left[2\sinh\left(\frac{\hbar\omega}{2k_B T}\right)\right] d\omega, \tag{2}$$

where ω=$\omega(V)$ depends on volume and thus Equation (2) contains some effect of anharmonics, and $g(\omega)$ is the phonon DOS which should be positive. So, this formula is not suitable for dynamically unstable phases. Instead, the Debye model can be employed to estimate the vibrational energy for phases with imaginary phonon frequencies by

$$F_{vib}(V,T) = \frac{9}{8}k_B\Theta_D + k_B T\left[3\ln(1-exp(-\frac{\Theta_D}{T}) - D(\frac{\Theta_D}{T})\right], \tag{3}$$

where $\frac{9}{8}k_B\Theta_D$ is the zero-point energy due to lattice ion vibration at 0 K, and $D(\frac{\Theta_D}{T})$ is the Debye function given by $D(\frac{\Theta_D}{T}) = \frac{3}{x^3}\int_0^{\Theta/T} x^3/(e^x-1)dx$ as introduced in Ref. [22] explicitly. F_{ele} in Equation (1) can be obtained from the energy and entropy contributions, *i.e.*, $E_{ele} - TS_{ele}$. The electronic entropy S_{ele} is of the form

$$S_{ele}(V,T) = -k_B \int n(\varepsilon,V)[f\ln f + (1-f)\ln(1-f)]d\varepsilon, \tag{4}$$

where $n(\varepsilon)$ is electronic DOS, and f is the Fermi-Dirac distribution. The energy E_{ele} due to the electron excitations takes the following form

$$E_{ele}(V,T) = \int n(\varepsilon,V) f \varepsilon d\varepsilon - \int^{\varepsilon_F} n(\varepsilon,V)\varepsilon d\varepsilon, \tag{5}$$

where ε_F is the Fermi energy.

The DFT calculations are carried out using the Vienna *ab initio* simulations package (VASP) [23, 24] with the projector-augmented-wave (PAW) potential methods [25]. The exchange and correlation effects are described by generalized gradient approximation (GGA) in the Perdew-Burke-Ernzerhof (PBE) form [26] and the plane-wave basis set is limited by the cutoff energy of 500 eV. The integration over the Brillouin Zone (BZ) is done on 18×18×16, 16×16×9, and 18×18×18 k-point meshes generated by the Monkhorst-Pack [27] method for α (two-atom cell), ω (six-atom 1×1×2 supercell), and β (two atoms cell) phases, respectively. Full geometry optimization at each volume is considered to be completed when the energy convergence and Hellmann-Feynman forces become less than 1.0×10^{-5} eV/atom and 0.01 eV/Å, respectively.

III. RESULTS AND DISCUSSIONS

A. Ground state properties

The total energies of the α, ω, and β phases at different volumes are calculated and shown in Fig. 1(a). Obviously, the ω phase is estimated to be the most stable structure, and the β phase most unstable. The energy-volume curve of α phase intersects with that of β and ω phases at different volumes respectively. The volumes of the three phases as a function of pressure are depicted in Fig. 1(b). Clearly, the volume of α phase is always the largest at the considered pressure range, while the volume-pressure curves of ω and β phases have an intersection at around −4.4 GPa. In order to obtain the theoretical equilibrium lattice parameter (a), bulk modulus (B), and pressure derivative of bulk modulus (B') of the three phases, we fit their energy-volume data to the third-order Birch-Murnaghan equation of states (EOS) [28]. The fitting results are tabulated in Table I, together with the experimental values [11, 29–37] for comparison. The corresponding data of pure Hf and Ti metals are also calculated and listed in Table I. Evidently, for α phase, one can find excellent coincidence between our calculated values and the corresponding experimental results of equilibrium

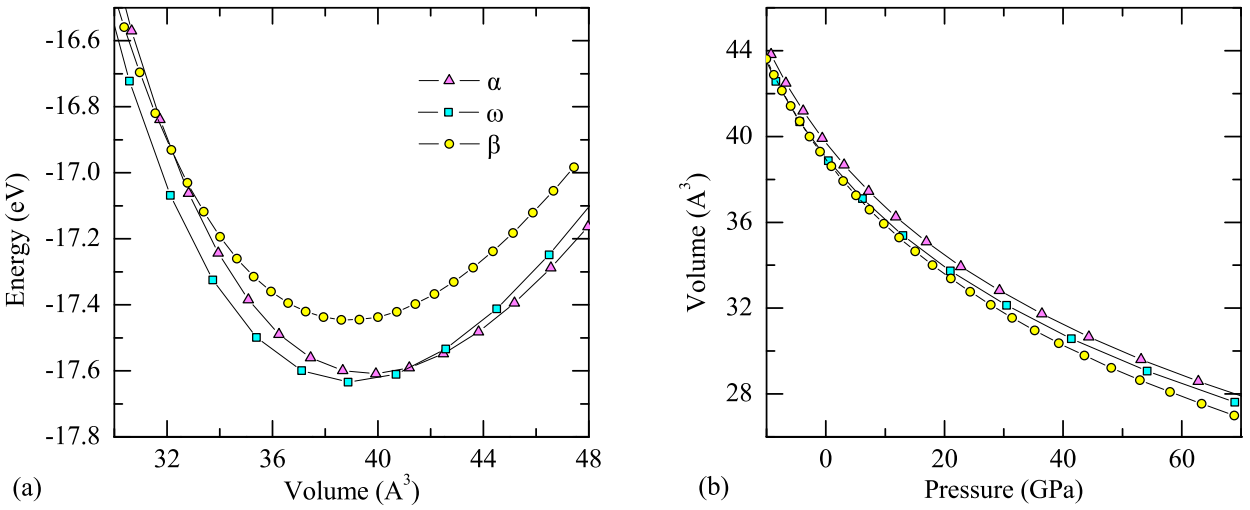

FIG. 1: Calculated (a) ground-state energy as a function of volume per formula unit cell, and (b) volume as a function of pressure for α, ω, and β HfTi alloy.

lattice parameters a and c/a ratio for both the alloy and the pure metals. The calculated bulk modulus B of 110.6 GPa for α-HfTi alloy lies within the range between α-Hf (108.2 GPa) and α-Ti (113.0 GPa). For the ω phase, our calculated equilibrium crystal constants of Hf and Ti are both in agreement with the corresponding experimental results within 1% error, and a value of 4.774 Å for their alloy is obtained. As for the high temperature β phase, our calculated lattice parameter of Hf is lower than the experimental value by 1.9 %, the reason of which can be attributed to the lattice thermal expansion with temperature. Similar to other two phases, the equilibrium lattice parameter of β-HfTi lies within the corresponding values of Hf and Ti.

B. Pressure induced phase transition

As shown in Fig. 1(a), the intersection of energy-volume curves between α phase and other two phases indicate that the phase transformation will occur between them at specific pressures. Theoretically, the transition pressure between α and ω phases can be obtained from the common tangent of their energy-volume curves. However, it is difficult to determine the slop accurately. Optionally, we can obtain the transition pressure by comparing their Gibbs free energy. At 0 K, the Gibbs free energy is equal to the enthalpy H=E+PV. In Fig. 2 we plot the enthalpies of the α and ω phases with respect to the β phase as a function of

TABLE I: Calculated lattice constants (a and c/a), bulk modules (B), pressure derivative of bulk modulus (B'), and elastic constants of α-, ω-, and β-phase HfTi, Hf, and Ti at ambient pressure. For comparison, experimental results are also listed.

	Phase	Method	a (Å)	c/a	B (GPa)	B'	C_{11} (GPa)	C_{12} (GPa)	C_{13} (GPa)	C_{33} (GPa)	C_{44} (GPa)
HfTi	α	This study	3.122	1.555	110.6	3.61	194.0	66.1	75.8	193.0	45.1
		Expt.	3.08	1.571[a,b]							
	ω	This study	4.774	0.619	117.8	3.07	194.9	81.8	58.3	245.2	49.9
	β	This study	3.402		107.5	3.26	99.5	120.8			38.9
Hf	α	This study	3.202	1.581	108.2	3.37	194.0	59.0	68.8	196.2	52.7
		Expt.	3.190	1.583[c,d]			190.1	74.5	65.5	204.4	60.0[e]
	ω	This study	4.989	0.621	109.3	3.45	200.3	76.4	47.6	240.4	49.1
		Expt.	4.943	0.617[f]							
	β	This study	3.545		95.5	3.58	72.5	115.1			51.8
		Expt.	3.615[g]								
Ti	α	This study	2.939	1.583	113.0	3.424	194.4	63.6	77.1	188.8	42.8
		Expt.	2.957	1.585	102.0	3.9[h]					
			2.95	1.586	114.0(3)	4.0[i]					
			2.951	1.587			162.4	92.0	69.0	180.7	46.7[j]
							176	86.9	68.3	191	50.8[e]
	ω	This study	4.580	0.618	111.5	3.51	195.9	84.6	55.0	243.6	53.3
		Expt.	4.598	0.614	142.0[h]						
	β	This study	3.25		105.7	3.33	93.6	115.9			39.8

[a] Ref. [29], [b] Ref. [30], [c] Ref. [31], [d] Ref. [32], [e], Ref. [33], [f] Ref. [34], [g] Ref. [35], [h] Ref. [11], [i] Ref. [37], [j] Ref. [36].

pressure. Clearly, at ambient pressure and above the ω phase is more stable than the α one, and there is no crossing between them. Indeed, in our calculation, the crossing between the ω and α enthalpy curves lies at the pressure of -4.3 GPa. This result is consistent with the theoretical result of Ti [14, 38], however, it is inconsistent with the transition sequence of Hf both experimentally and theoretically [9, 39–41]. To further investigate the phase stability,

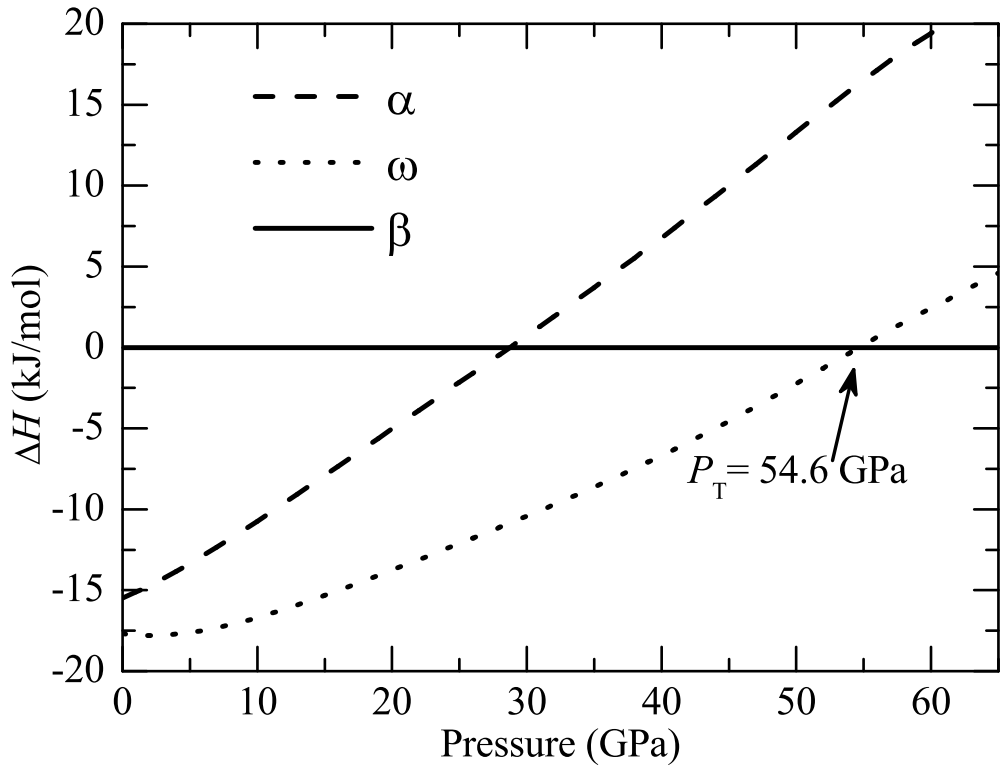

FIG. 2: Calculated enthalpy differences of α and ω phases with respect to β phase as a function of pressure.

in Table II we list the transition pressures for HfTi alloy as well as for pure Hf and Ti metals from both experiments and theoretical calculations. For metal Hf, at ambient pressure both the experimental [9] and theoretical studies [39–41] indicate that the most stable phase is the α phase. The measured transition pressure of $\alpha \rightarrow \omega$ is 38$\pm$8 GPa [9], and the theoretical results vary from 13.9 GPa [39] to 43.5 GPa [40] and 44.5 GPa [41]. For metal Ti, there exist debates in theoretical studies [14, 38, 42], although experiments [10–13] have reported the most stable phase to be α phase, as shown in Table II. We find that the theoretical DFT-PBE studies [14, 38], giving the negative $\alpha \rightarrow \omega$ transition pressures, are performed at 0 K. While, by considering the temperature, the DFT-PBE study [43] explicitly show that the $\alpha \rightarrow \omega$ transition occurs at $\sim$1.8 GPa at room temperature. Thus, the disagreement between some theoretical studies and measured values for Ti metal mainly originates from the effect of temperature. For HfTi alloy, the phase transition of $\omega \rightarrow \beta$ occurs at 54.6 GPa. This value coincides with the theoretical results of 30.7-66.2 GPa [39–41] for Hf metal, and is somewhat lower than the experimental data of 71 GPa [9]. Also, the temperature effect

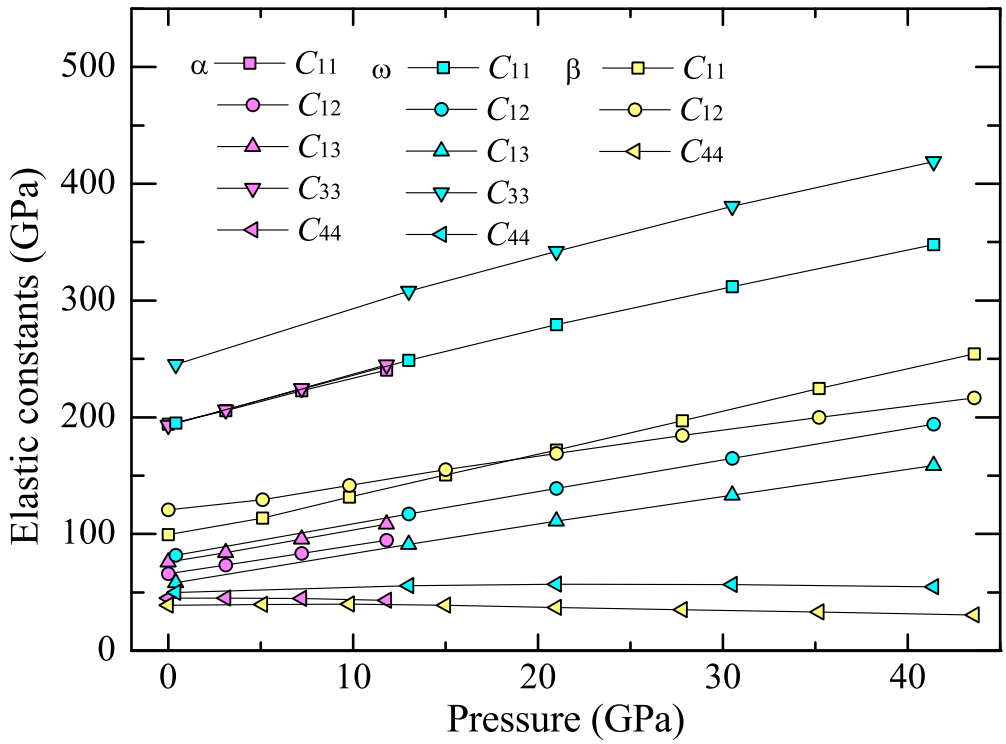

FIG. 3: Calculated elastic constants as a function of pressure for α, ω, and β HfTi alloy.

on phase transition pressure cannot be ignored. Thus, here we will consider the effect of temperature on the transition sequence of HfTi alloy by employing the same scheme as in our previous studies of Zr metal [44] and TiZr alloy [45].

C. Elasticity behavior at high pressure

Elastic constants not only provide valuable information about the bonding characteristic between adjacent atomic planes and anisotropy in the bonding, but also can measure the resistance and mechanical features of crystal to external stress or pressure, which further describe the stability of crystals against elastic deformation. Our calculated results of the elastic constants for the three phases of HfTi alloy are listed in Table I. For comparison, the theoretical and experimental results of pure Hf and Ti metals are also listed. Evidently, the α and ω phases for HfTi alloy as well as the pure Hf and Ti metals are all mechanically stable at ambient pressure. However, the β phase is unstable for both HfTi alloy and its archetype metals, since their elastic constants do not satisfy the mechanical stability criteria of cubic structure [46]. In general, for α and ω HfTi alloy, our calculated values of the five

TABLE II: Calculated transition pressure of HfTi. For comparison, other theoretical results and experimental data for Hf and Ti are listed.

	Phase transition	Theory (GPa)	Expt. (GPa)
HfTi	$\alpha \rightarrow \omega$	-4.3[a]	
	$\omega \rightarrow \beta$	54.6[a]	
Hf	$\alpha \rightarrow \omega$	13.9[b], 43.5[c], 44.5[d]	38±8[e]
	$\omega \rightarrow \beta$	30.7[b], 62.6[c], 66.2[d]	71[e]
Ti	$\alpha \rightarrow \omega$	-3.7[f], -3.0[g], 52[h]	2-11.9[i]

[a] This study, [b] Ref. [39], [c] Ref. [40], [d] Ref. [41], [e] Ref. [9], [f] Ref. [14], [g] Ref. [38], [h] Ref. [42], [i] Refs. [10–13]

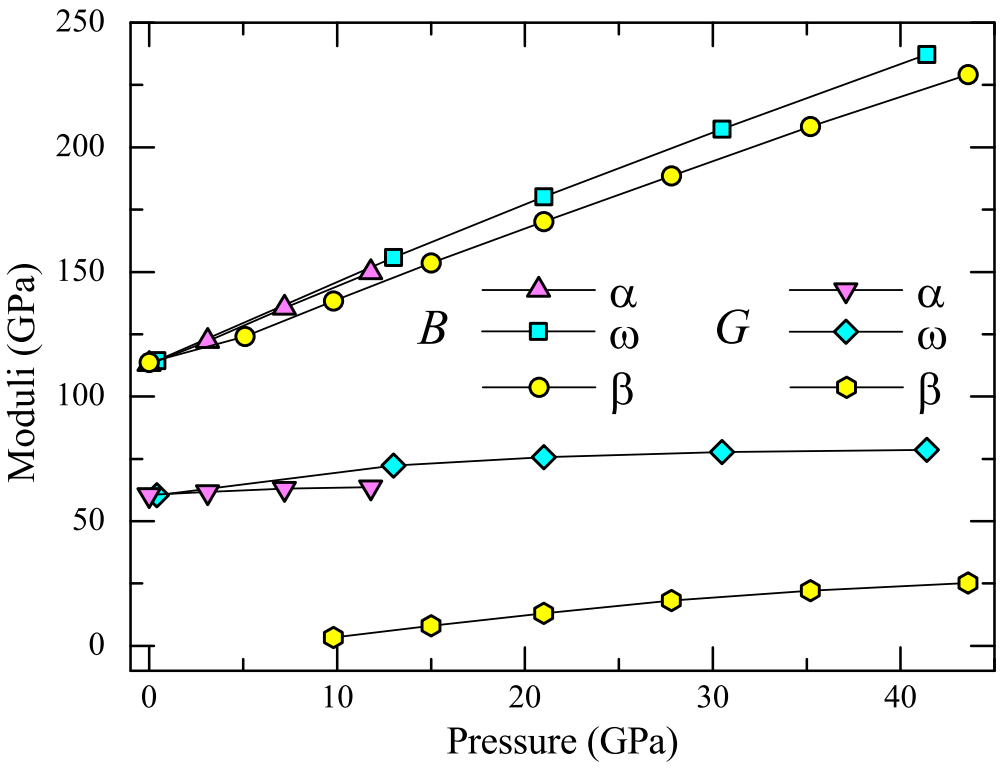

FIG. 4: Calculated bulk modulus (B) and shear modulus (G) as a function of pressure for α, ω, and β HfTi alloy.

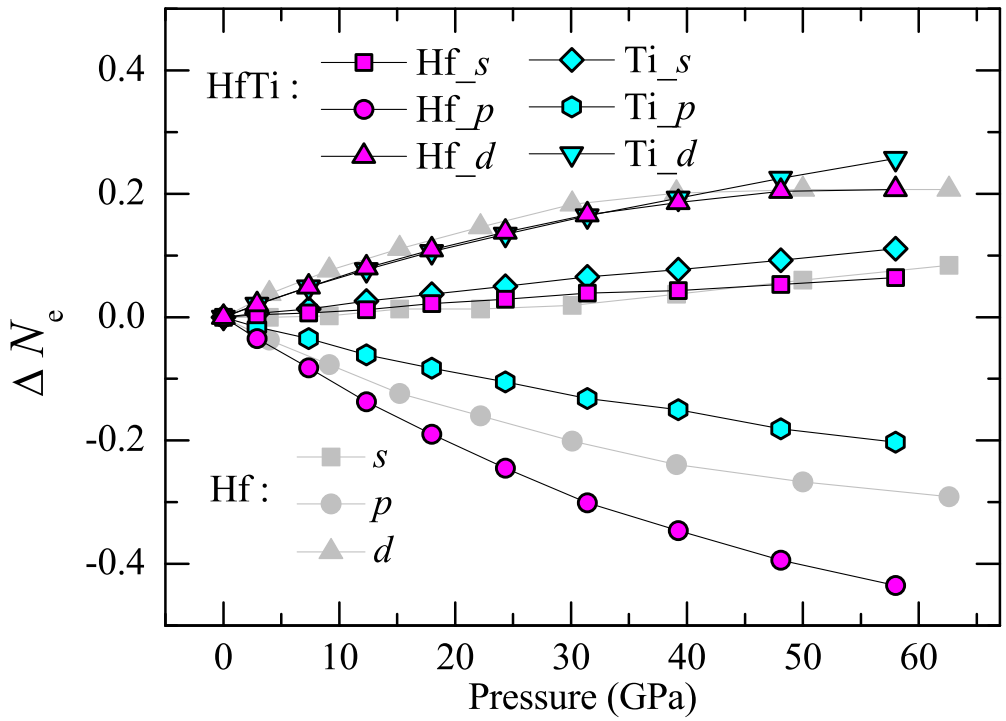

FIG. 5: The number of electrons on s, p, and d orbitals for β phase HfTi alloy and Hf metal as functions of pressure, with respect to to their values at ambient pressure.

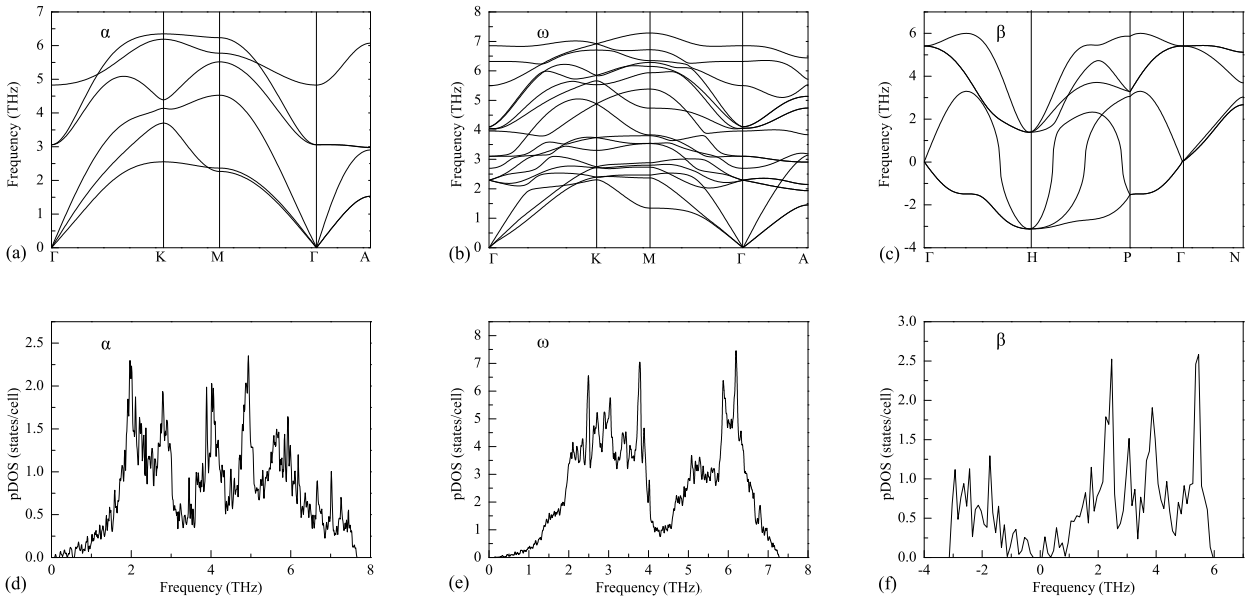

FIG. 6: Calculated Phonon dispersions (upper panels) and phonon DOS (lower panels) of α, ω, and β phases of HfTi alloy.

independent elastic constants at ambient pressure lie in the range of corresponding Hf and Ti metals. With increasing pressure, all the five elastic constants increase monotonically, among which the C_{44} has a moderate increase, while other four parameters increase rapidly with applied pressure, as shown in Fig. 3. We notice that parameter C_{33} of ω phase is much larger than C_{11}, indicating that the bonds between the nearest neighbors along the (001) plane are much stronger than the (100) plane. As for β-HfTi, the value of $C_{11}-C_{12}$ is negative, coinciding with that of Hf and Ti metals. As the pressure increases from 0 to 44 GPa, the values of C_{11} and C_{12} increase near linearly, and $C_{11}-C_{12}$ becomes positive at 18.5 GPa, as shown in Fig. 3.

After obtaining elastic constants at different pressures, the polycrystalline bulk modulus B and Shear modulus G as functions of pressure can be evaluated from the Voigt-Reuss-Hill (VRH) approximation [47–49], and the results are depicted in Fig. 4. For all the three phases of HfTi, the deduced bulk moduli from VRH approximation at ambient pressure turn out to be very close to that obtained from the EOS fitting, indicating that our calculations are consistent and reliable. As the pressure increases, both bulk modulus and shear modulus increase monotonically for all the three phases. The increasing rates of bulk moduli for all the three phases are apparently larger than that of shear moduli. It is well known that a high (low) ratio of B/G is responsible for the ductility (brittleness) of polycrystalline materials. Our calculated values of B/G for α phase increase from 1.86 to 2.36 under pressure from 0 GPa to 12 GPa, for ω phase increase from 1.89 to 3.02 with pressure enhancing from 0 to 42 GPa, for β phase decrease from 16.01 to 9.10 upon compression from 18.5 GPa to 44.0 GPa. Results show that transition to ω phase or β phase from α phase will enhance the ductility, and the β phase possess the biggest ductility. Our calculated B/G for α and ω phases are 1.62 and 1.66 for Hf, 1.89 and 1.75 for Ti, respectively. We notice that for the HfTi alloy the ductility is improved with respect to the pure Hf and Ti metals.

To discuss the pressure induced $s-d$ electron transfer, we perform the Mulliken charge population analysis [50] of the β phase. The variation of the number of electrons on s, p, d orbitals with increasing pressure for HfTi alloy and Hf metal are shown in Fig. 5. It is evident that the $s-d$ electron transfer behavior of HfTi and Hf are consistent. Upon compression up to 58 GPa, the d electrons of Hf and Ti atoms in HfTi alloy decrease, while the s and d electrons increases. This fact is the same as that in Hf metal. The increase of d-band occupancy will stabilize β phase of HfTi alloy under pressure.

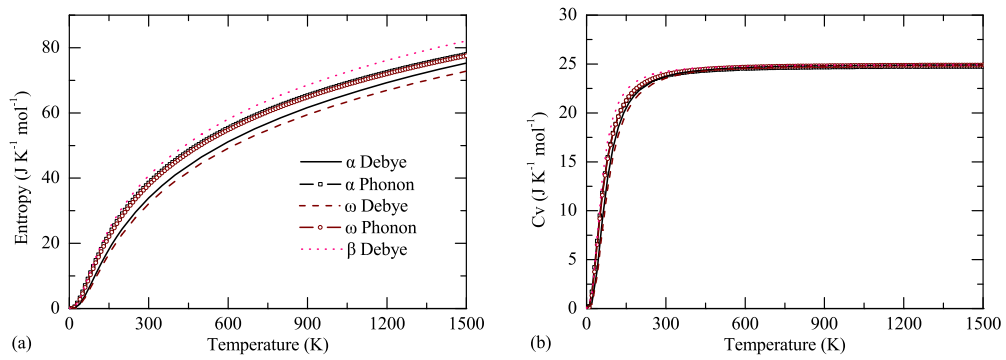

FIG. 7: Temperature dependence of (a) entropy and (b) specific heat at constant volume for α, ω, and β phases of HfTi alloy.

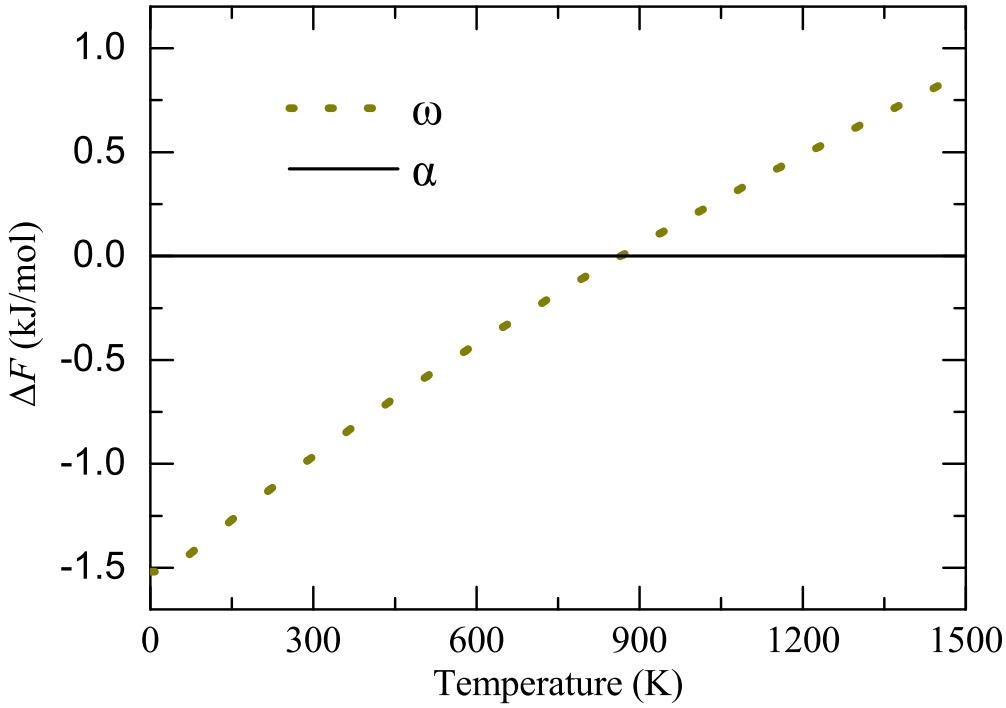

FIG. 8: The Helmholtz free energy difference (ΔF) of ω phase HfTi alloy with respect to α as a function of temperature by quasiharmonic approximation at ambient pressure.

D. The $P-T$ phase diagram

The vibration energy of lattice ions can be determined by the quasiharmonic approximation or the Debye model as specified in Sec II. In calculating the phonon dispersion curves and the phonon DOS, the Hellmann-Feynman theorem and the direct method [51] are employed. For the BZ integration, the 5×5×5, 3×3×1, and 5×5×5 k-point meshes are used

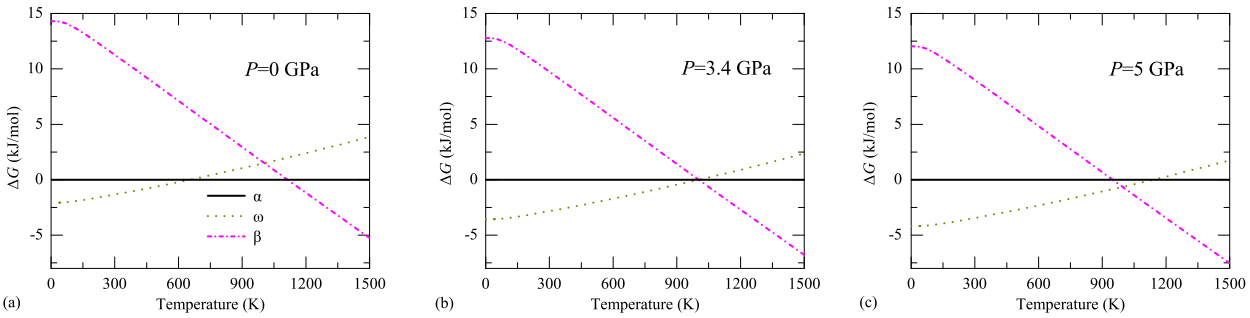

FIG. 9: Temperature dependence of the Gibbs free energy difference (ΔG) of HfTi phases with respect to α at different pressures, i.e., 0 GPa, 3.4 GPa, and 5 GPa.

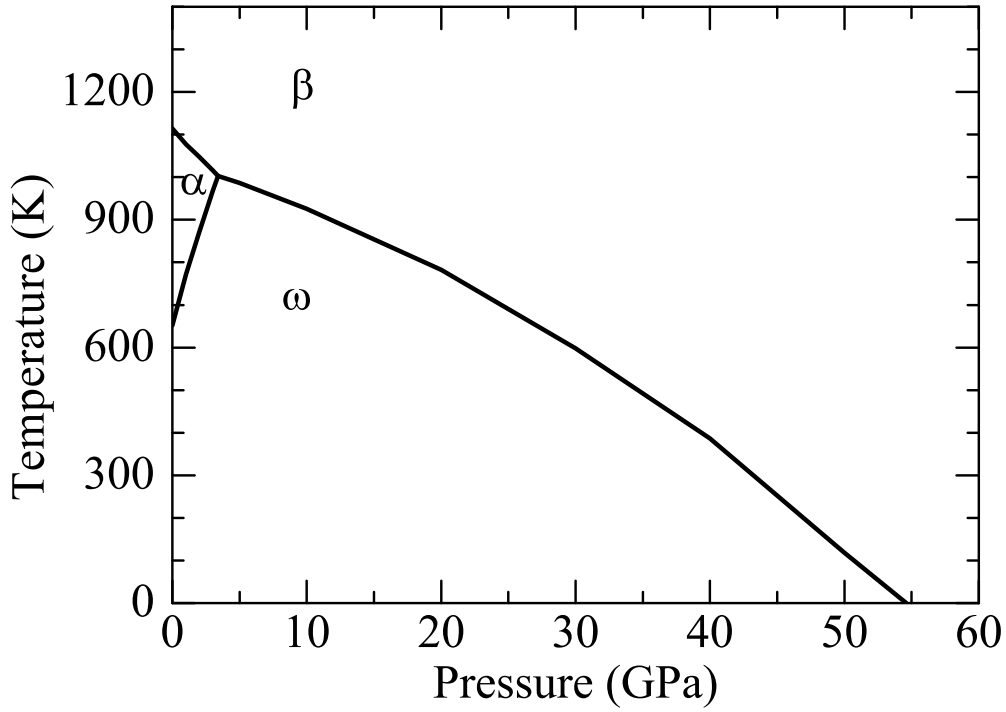

FIG. 10: $P-T$ phase diagram of HfTi alloy. The solid lines show our predicted $\alpha\rightarrow\omega$, $\omega\rightarrow\beta$, and $\alpha\rightarrow\beta$ transition boundaries by Debye model.

for the α, ω, and β 3×3×3 supercells, respectively. In Fig. 6 we show the calculated phonon dispersion curves and phonon DOS of α, ω, and β HfTi at ambient pressure. Obviously, the phonon dispersions of α and ω phases are stable at ambient pressure, while the β phase is unstable. The phonon behavior of α-HfTi is similar to that of metal Hf [52] and Ti [43]. There are obvious interactions between acoustic and optical branches in metal Hf and Ti. However, this character does not appear in their α phase alloy. The interaction between

Hf and Ti atoms in HfTi alloy is weaker than that in its archetype metals. Due to the low c/a ratio of the ω phase, the acoustic phonon branches of Ti metal are stiffer along the c axis than in the basal plane [43], and the HfTi alloy shows the same characteristics. As for the β phase, the only stable phonon branch is along [110] direction in HfTi alloy, which is different from that in metal Ti. The stable nature of phonon branch along [110] direction for β-HfTi indicates that the occurrence of phase transform from α or ω phase to β phase need considerable external driving force, such as high-temperature or high-pressure, to break the original phase structure.

The Gibbs free energy, the entropy, and the specific heat at constant volume (C_v) can be evaluated by both the quasiharmonic approximation and the Debye model. The entropies of α and ω phases obtained by quasiharmonic approximation are both somewhat higher than those obtained by Debye model, as shown in Fig. 7(a). The calculated C_v with quasiharmonic approximation is almost identical to that obtained by Debye model for α phase, while the difference between these two schemes for ω phase is slightly larger [Fig. 7(b)]. At ambient pressure the Gibbs free energy is equal to the Helmholtz free energy. As shown in Fig. 8, we calculate the Helmholtz free energy of ω phase with respect to the α phase as a function of temperature by quasiharmonic approximation. Note that the free energy calculations include the zero-point energy (2.483 kJ/mol for ω phase and 2.444 kJ/mol for α phase). A ω to α phase transition temperature of 865 K can be obtained. Since the β phase is thermodynamically unstable, we are unable to predict the lattice vibrational energy of the β phase by phonon DOS. Alternatively, we calculate the Gibbs free energy by the Debye model. Figure 9 shows the calculated Gibbs free energy of ω and β phases with respect to the α phase as a function of temperature at different pressures, *i.e.*, 0 GPa, 3.4 GPa, and 5 GPa. At zero pressure the ω phase has the lowest Gibbs energy within the temperature range 0 K$<T<$653 K, and this transition temperature is lower than that deduced from quasiharmonic approximation by $\sim$200 K. From 653 K to 1112 K, the α phase is preferred, and this result is consistent with the experimental temperature range of 500-1165 K [18]. When the temperature is further increased to be beyond 1112 K, the β phase becomes stable. At P=3.4 GPa, the three phases have the same Gibbs energy at 1003 K, corresponding to a triple point in the $P-T$ phase diagram. Above 3.4 GPa, the ω phase transits to β phase without formation of α phase [Fig. 9(c)]. Finally, in Fig. 10 we depict the $P-T$ phase diagram of HfTi alloy calculated by Debye model. Remarkably, our

calculated $\alpha \rightarrow \beta$ transition temperature at ambient pressure (1112 K) is very close to the experimental measurement (1203±31 K) [53]. The triple point is predicted to be (3.4 GPa, 1003 K), which needs experimental test to identify in the future.

IV. CONCLUSIONS

In summary, the structural phase transition, pressure-dependent elasticity behavior, and phonon spectra of HfTi alloy have been theoretically studied. The obtained ground-state structural parameters of α and ω phases of HfTi alloy and its archetype metals are consistent well with accessible experimental data. The calculated elastic constants indicate that the α and ω phases are mechanically stable at ambient pressure, while the β phase is unstable. The values of elastic constants for all the three phases of HfTi alloy are between Hf and Ti metals. The $\alpha \rightarrow \beta$ alloy phase transition pressure is predicted to be 54.3 GPa, which is close to that for Hf metal. Under compression, elastic constants, bulk modulus B, and shear modulus G increase almost linearly for all the three phases. The β phase become mechanically stable at 18.5 GPa. The Mullikey charge population analysis shows that the p electrons of Hf and Ti in β HfTi alloy transfer to corresponding d and s orbitals upon compression, which strengthens the stability of β phase under pressure, and this character is similar to that in β-Hf metal. The nature of stability for α and ω phases at ambient pressure has also been observed from phonon dispersions. As for the β phase, the only stable phonon branch is along the [110] direction, which is different from that in metal Ti. The lattice vibrational energy was calculated based on quasiharmonic approximation from both the phonon DOS and Debye model. As a consequence, thermodynamic properties of Gibbs free energy, entropy, and specific heat at constant volume of α- and ω-HfTi have been theoretically obtained. The transition temperature of $\omega \rightarrow \alpha$ at ambient pressure is 865 K by phonon and 653 K by Debye model, respectively. Finally, based on the Gibbs free energy evaluated from Debye model as functions of pressure and temperature, the $P-T$ phase diagram has been depicted. Remarkably, our predicted $\alpha \rightarrow \beta$ phase transition temperature of 1112 K coincides well with the attainable experimental report.

Acknowledgments

This work was supported by NSFC under Grant No. 51071032, and by Foundations for Development of Science and Technology of China Academy of Engineering Physics under Grants No. 2011A0301016.

---

[1] J. H. Schemel, ASTM Manual on Zirconium and Hafnium. ASTM International, 1-5, ISBN 9780803105058, (1977).

[2] J. B. Hedrick, United States Geological Survey, Retrieved (2008-09-10).

[3] D. Spink, Ind. Eng. Chem., **53**(2), 97 (1961).

[4] M. J. Donachie, ASTM International, 235-236, ISBN 9780871707499, (2002).

[5] J. C. Duthie, D. G. Pettifor, Phys. Rev. Lett. **38**, 564 (1977).

[6] H. L. Skriver, Phys. Rev. B **31**, 1909 (1985).

[7] R. S. Hixson, D. A. Boness, J. W. Shaner, and J. A. Moriarty, Pliys. Rev. Lett. **62**, 637 (1989).

[8] Y. K. Vohra, and A. L. Ruoff, Phys. Rev. B **42**, 8651 (1990).

[9] H. Xia, G Parthsarthy, H Luo, Y. K. Vohra and A. Ruoff, Phys. Rev. B **42**, 6736 (1990).

[10] H. Xia, S. J. Duclos, A. L. Ruoff, Y. K. Vohra, Phys. Rev. Lett. **64**, 204 (1990).

[11] Y. K. Vohra, P. T. Spencer, Phys. Rev. Lett. **86** 3068 (2001).

[12] Y. Akahama, H. Kawamura, T. LeBihan, Phys. Rev. Lett. **87**, 275503 (2001).

[13] D. Errandonea, Y. Meng, M. Somayazulu, D. Häusermann, Physica B **355**, 116 (2005).

[14] Z. G. Mei, S. L. Shang, Y. Wang and Z. K. Liu, Phys. Rev. B **79**, 134102 (2009).

[15] A. K. Verma, P. Modak, R. S. Rao, B. K. Godwal, R. Jeanloz, Phys. Rev. B **75**, 014109 (2007).

[16] A. G. Imgram, D. N. Williams and H. R. Ogden, J. Less-Common Metals, **4**, 217 (1962).

[17] J. L. Murray, Bull. Alloy Phase Diagrams **2**, 181 (1981).

[18] H. Bittermann and P. Rogl, J. Phase Equilib. **18**, 1 (1997).

[19] E. T. Hayes and D. K. Deadorff, U.S. At. Energy Comm., Tech. Report No. USBM-V-345 (1957).

[20] M. A. Tylkina, A. I. Pekarev, and E. M. Savitskii, Zh. Neorg. Khim. **4**(10), 2320 (1959) in Russian; TR: Russ. J. Inorganic Chem. **4**(10), 1059 (1959).

[21] A. Siegel, K. Parlinski, and U. D. Wdowik, Phys. Rev. B **74**, 104116 (2006).

[22] A. A. Blanco, E. Francisco, and V. Luana, Comput. Phys. Commun. **158**, 57 (2004).

[23] G. Kresse, J. Furthmüller, computer code VASP, Vienna, (2005).

[24] G. Kresse, J. Furthmüller, Phys. Rev. B **54**, 11169 (1996).

[25] P. E. Blöchl, Phys. Rev. B **50**, 17953 (1994).

[26] J. P. Perdew, K. Burke and M. Ernzerhof, Phys. Rev. Lett. **77**, 3865 (1996).

[27] H. J. Monkhorst, J. D. Pack, Phys. Rev. B **13**, 5188 (1976).

[28] F. Brich, Phys. Rev. **71**, 809 (1947).

[29] Y. A. Chang, U.S.A.F. Tech. Rep. AFML-TR-65-2, Part II, Vol. V (1966).

[30] E. Rudy, AFML-TR-65-2, (1969)

[31] C. Kittel, Introduction to Solid State Physics, Wiley, New York, (1971).

[32] J. Donohue, The Structures of the Elements, Wiley, New York, (1974).

[33] E. S. Fisher and C. J. Renken, Phys. Rev. **135**, A482 (1964).

[34] S. K. Sikka, Y. K. Vohra and R. Chidambaram, Prog. Mater Sci. **27**, 245 (1982).

[35] E. Y. Tonkov and E. G. Ponyatovsky, Phase Transformations of Elements Under High Pressure, CRC Press, Boca Raton, FL, (2005).

[36] S. A. Ostanin, V. Y. Trubitsin, J. Phys.: Condens. Matter **9**, L491 (1997).

[37] J. Z. Zhang, Y. Zhao, R. S. Hixson, G. T. Gray, L. P. Wang, W. Utsumi, S. Hiroyuki, and H. Takanori, Phys. Rev. B **78**, 054119 (2008).

[38] A. L. Kutepov and S. G. Kutepova, Phys. Rev. B **67**, 132102 (2003).

[39] R. Ahuja, J. M. Wills, B. Johansson, and O. Eriksson, Phys. Rev. B **48**, 16269 (1993).

[40] G. Jomard, L. Magaud and A. Pasturel, Phil. Mag. B **77**, 67 (1998).

[41] Y. J. Hao, J. Zhu, L. Zhang, H. S. Ren, and J. Y. Qu, Phil. Mag. Lett. **91**, 61 (2011).

[42] F. Jona, P. M. Markus, Phys. Stat. Sol. (b) **242**, 3077 (2005).

[43] Z. G. Mei, S. L. Shang, Y. Wang, Z. K. Liu, Phys. Rev. B **80**, 104116 (2009).

[44] B. T. Wang, P. Zhang, H. Y. Liu, W. D. Li, P. Zhang, J. Appl. Phys. **109**, 063514 (2011).

[45] B. T. Wang, W. D. Li, and P. Zhang, J. Nucl. Mater., **420**, 501 (2012).

[46] J. F. Nye, Physical Properties of Crystals (Oxford University Press, Oxford, 1985).

[47] W. Voigt, Lehrburch der Kristallphysik, Teubner, Leipzig, (1928).

[48] A. Reuss, Z. Angew. Math. Mech. **9**, 49 (1929).

[49] R. Hill. Phys. Soc. London **65**, 350 (1952).

[50] R. S. Mulliken, J. Chem. Phys. **23**, 1833 (1955).

[51] K. Parlinski, Z. Q. Li, Y. Kawazone, Phys. Rev. Lett **78**, 4063 (1997).

[52] R. P. Bajpai, Physica, **62**, 574 (1972).

[53] G. I. Ruda, I. I. Kornilov, and V.V. Vavilova, lzv. Akad. Nauk SSSR Met. **5**, 203 (1975) in Russian; TR: Russ. Met. **5**, 160 (1975).